Journal of Electron Spectroscopy and Related Phenomena 185 (2012) 567–572

Contents lists available at SciVerse ScienceDirect

Journal of Electron Spectroscopy and Related Phenomena

journal homepage: www.elsevier.com/locate/elspec

Growth of nano Co encapsulated in carbon-shell

H.Y. Kang[a], H. Paul Wang[a,b,c,*], W.-K. Lin[d], I-W. Sun[e], C.-J.G. Jou[f], U-Ser Jeng[g], S.G. Chang[h]

[a] Department of Environmental Engineering, National Cheng Kung University, Tainan 70101, Taiwan
[b] Sustainable Environmental Research Center, National Cheng Kung University, Tainan 70101, Taiwan
[c] Center for Micro/Nano Science and Technology, National Cheng Kung University, Tainan 70101, Taiwan
[d] Department of Engineering and System Science, National Tsing-Hua University, Hsin Chu 30013, Taiwan
[e] Department of Chemistry, National Cheng Kung University, Tainan 70101, Taiwan
[f] Department of Safety Health and Environmental Engineering, National Kaohsiung First University of Science & Technology, Kaohsiung 81164, Taiwan
[g] National Synchrotron Radiation Research Center, Hsin Chu 30076, Taiwan
[h] Environmental Energy Technologies Division, Lawrence National Berkeley Laboratory, Berkeley, CA 94720, USA

ARTICLE INFO

Article history:
Received 21 September 2012
Received in revised form
15 November 2012
Accepted 15 November 2012
Available online 23 November 2012

Keywords:
Core-shell nanoparticle
Cobalt
Magnetic properties
SAXS
XANES

ABSTRACT

Nanostructured cobalt is one of the key elements in catalysis and therapeutic drug delivery. To design and prepare nanosize-controllable cobalt, a better understanding of its growth mechanism is essential. Growth of Co nanoparticles encapsulated in carbon-shell (Co@C) during temperature-programmed carbonization of the Co^{2+}-β-cyclodextrin (CD) complex at 363–573 K was, therefore, studied by *in situ* synchrotron small-angel X-ray scattering and X-ray absorption near edge structure spectroscopy. The carbon-shell having a thickness of about 2 nm can prevent the core Co from being aggregated and oxidized. A relatively slow reduction of Co(II) to Co is observed at 393–423 K (stage I) prior to a particle growth transition-state possessing Co of 2.2 nm in diameter at 423–483 K. At 483–513 K (stage II), an increasing Co(II) reduction rate coupled with a rapid fusion and coalescence of Co nanoparticles is found. The average growth rates of Co at stages I and II are about 27 and 98 atoms/min, respectively. The most-probable particle diameter of the ripened Co is 5.9 nm. The carbon-shell can be removed by steam reforming to yield the Co nanoparticles. This work also exemplifies the possible temperature-controllable growth of Co@C, especially in the Co size range of 2–6 nm in diameter.

© 2012 Elsevier B.V. All rights reserved.

1. Introduction

Nanostructured cobalt compounds have been widely used in catalysis [1]. $CoFe_2O_4$ nanoparticles functionalized with -NH_2 can be used in drug delivery [2]. The physicochemical properties of nanosized metallic cobalt (Co) can be modified by surface coatings with polymers, carbon, or silica [3,4]. The carbon coating on Co nanoparticles (Co@C) are of great interest because carbon has a high thermal and chemical stability [5–13]. The carbon-shell may protect the core Co nanoparticles from being oxidized or aggregated, and also improve their dispersion or compatibility in solutions or on substrates [14–17]. Notably, Co@C can be designed to be functionalized as nanoreactors for enhancing collision frequencies in the confined space [18].

Co nanoparticles may cause cell lysis and death *via* DNA fragmentation [19]. The magnetic Co nanoparticles also possess a strong heating effect that can be utilized for the hyperthermia cancer therapy and *in vitro* diagnostics of magnetic resonance imaging (MRI) [20–24]. The carbon-shell can enhance the relaxation of water proton and hence increase the MRI contrast as well as the penetration of Co@C into cell nucleus [25]. However, the magnetic and thermal activation properties of the Co nanoparticles are dependent on their shape, size, and nanostructure, which need to be carefully controlled for practical biomedical applications [26].

The composition and chemical structure of Co-Ni nanoparticles synthesized by chemical co-reduction of Co(II) and Ni(II) in a sodium-phosphate matrix could be controllable by the chemical reduction sequence [27]. The growth rate and morphology of nanosized CoPt thin films (2 nm in thickness) prepared by pulsed laser deposition on carbon and Al_2O_3 substrates was found relating to the laser frequency and substrate temperature [28]. Cobalt nanoparticles grown on carbon-coated substrates by atomic vapor deposition might be proceeded with nucleation, absorbing the smallest particles into adjacent large one, and then rapid particle fusion and coalescence into a single Co nanoparticle [29]. The challenge is to develop a method that allows the preparation of Co nanoparticles with a desirable size as catalytic active sites. To facilitate such a development, it would be very important to understand the growth mechanism of Co particles.

* Corresponding author at: Department of Environmental Engineering, National Cheng Kung University, Tainan 70101, Taiwan. Tel.: +886 6 276 3608; fax: +886 6 275 2790.
E-mail address: wanghp@mail.ncku.edu.tw (H.P. Wang).

0368-2048/$ – see front matter © 2012 Elsevier B.V. All rights reserved.
http://dx.doi.org/10.1016/j.elspec.2012.11.010

Generally, nanosized metal active species prepared by known methods have limited size and dispersion and are susceptible to oxidation or aggregation. A shell of cobalt oxides (CoO or $CoCO_3$) could be formed on the surface of Co nanoparticles leading to a core-shell structure of Co@CoO/$CoCO_3$ [30]. In separate experiments, a simple method for preparing nanosize-controllable core-shell materials such as Cu@C, Ag@C and other metals or bimetals encapsulated in carbon-shell has been developed [31,32]. By carbonization at elevated temperatures, core-shell nanoparticles can be prepared in a single process. It is worth noting that the carbon-shell which can protect the core metals from being oxidized or aggregated can be removed by steam reforming ($C + H_2O \rightarrow CO + H_2$) if needed. In the present work, the growth mechanism of Co nanoparticles was studied by *in situ* small angle X-ray scattering (SAXS) and X-ray absorption near edge structure (XANES) spectroscopy. Specifically, the size, shape, and speciation of the Co nanoparticle encapsulated in carbon-shell were studied during temperature-programmed carbonization (TPC) of the Co^{2+}-β-cyclodextrin complex at the temperature range of 363–573 K. The future applications of the prepared Co@C may be further investigated with its photo-thermal characteristics and tailored for the use of eradicating malignant tumors.

2. Experimental

The Co@C nanoparticles were prepared by the method developed in our laboratory [31]. Briefly, cobalt(II) nitrate (purity 98%, Sigma-Aldrich) and β-cyclodextrin (CD) (purity 97%, Wako) were dissolved in distilled water at a Co/CD molar ratio of 6. The well mixed solutions were dried at 333 K to form the Co^{2+}-CD complex powder. The complex powder was carbonized in high-purity nitrogen atmosphere at 573 K for 2 h to yield Co@C core-shell nanoparticles. Steam reforming of the Co@C was carried out under 5% of steam in a stream of high-purity N_2 gas (a flow rate of 70 mL/min) at 573 K for 10 minutes to remove the carbon shell ($C + H_2O \rightarrow CO + H_2$).

The thermogravimetric analyses (TGA, SDT Q600, Thermal Advantage) coupled with a Fourier transform infrared spectroscopy (FTIR, Nicolet 6700, Thermo Scientific) (TGA-FTIR) were carried out to monitor weight loss of the Co^{2+}-CD complexes and product gases evolved during TPC. Samples of *ca.* 8 mg were heated from 298 to 600 K at a heating rate of 5 K/min in high-purity N_2 gas under a flow rate of 100 mL/min. FTIR spectra were recorded in the spectral range of 400–4000 cm^{-1} with a resolution of 4 cm^{-1} and 32 scans per second under a transmission mode.

The transmission electron microscopy (TEM) images of the Co@C nanoparticles were obtained on a microscope (JEM-3010, JEOL) operated at an acceleration voltage of 200 kV. The magnetic properties of the Co@C samples were measured using a superconducting quantum interference device vibrating sample magnetometer (SQUID VSM, Quantum Design MPMS). The field dependence of the static (DC) magnetization M (H) and the hysteresis curves were determined at 300 K in the applied external magnetic fields ranged from -2 to 2 T.

The *in situ* synchrotron SAXS measurements were performed on the beamline 23 A SWAXS at the Taiwan National Synchrotron Radiation Research Center (NSRRC). The storage ring was operated at 1.5 GeV and 300 mA. The beam was selectively monochromated by a double Mo/B_4C-multilayer monochromater with a modest energy resolution ($\Delta E/E = 1 \times 10^{-2}$ eV/eV) under the energy of 14 keV. During TPC, the Co^{2+}-CD complex powder samples were placed in the sample holder, and heated from 298 to 573 K at a heating of 5 K/min under flowing high-purity nitrogen gas (100 mL/min) [33]. The particle sizes of the sample were fitted by the SAXS patterns with the Schultz distribution function after removing contributions of the background, analyzed by the TableCurve softeware (Jandel scientific) as polydisperse spheres between q range of 0.01–0.09 $Å^{-1}$, where q is the magnitude of the scattering vector [34–36]. The errors of the most-probable particle size (d_p) in diameter (nm) were obtained by statistics of three data sets.

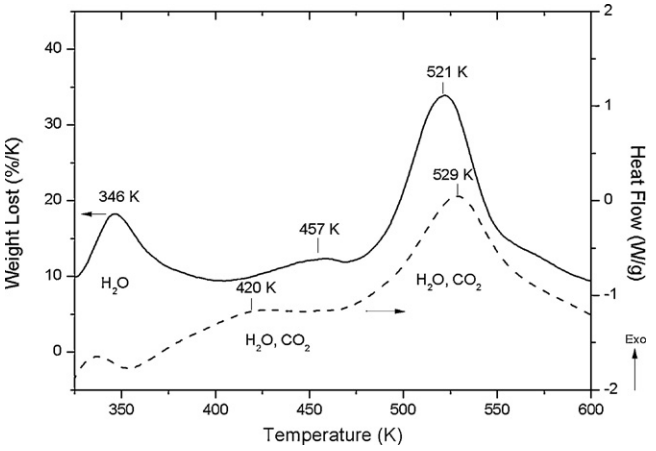

Fig. 1. Thermal gravimetric analyses for temperature-programmed carbonization of the Co^{2+}-CD complexes. The evolved gaseous compounds were monitored by on-line FTIR.

The XANES spectroscopic studies were carried out on the Wiggler beamline BL17 C at NSRRC. The storage ring was operated at 1.5 GeV and 300 mA. A Si(111) double-crystal monochromator was used to select the beam energy with an energy resolution of $\Delta E/E$ of 1.9×10^{-4} eV/eV. The XANES spectra of a sample is obtained by scanning with synchrotron X-ray radiation at the range of -40 to +60 eV at the absorption edge of Co K edge (7709 eV) with the data collected at steps of 0.4 eV in transmission mode by a Lytle detector at room temperature in atmosphere. The photon energy was calibrated with a standard Co foil. The standard deviation calculated from the averaged spectra was used to estimate the statistical noise and error associated with each structural parameter. XANES spectra of standard Co compounds having various oxidation states that may be possibly found in our sample, *e.g.*, Co, CoO, Co_2O_3, Co_3O_4, and $CoCO_3$ were also collected. The X-ray absorption data were analyzed using the IFEFFIT software package [37]. The fractions of Co species in a sample was obtained by linear-component fitting of the XANES spectrum of a sample with the XANES spectra of standard Co species having various oxidation states, with R-factor <0.002. Three replications of the *in situ* synchrotron SAXS and XANES measurements were taken.

3. Results and discussion

The TGA and related heat flow curves for TPC of the Co^{2+}-CD complex are shown in Fig. 1. H_2O is evolved at 325–400 K with a peak centered at 350 K, which is associated with the dehydration of the Co^{2+}-CD complex. At the temperatures of 400–600 K, a continuing evolution of CO_2 together with H_2O vapor is observed, suggesting oxidation of the–CH_2-O-CH(-OH)-C- groups in CD. Note that at 500–550 K, an intense endothermic peak with high weight loss is observed, which may be associated with the rapid oxidation coupled with reduction (*i.e.*, Co^{2+} to Co). Since neither CO_2 nor H_2O is formed from TPC at 573 K, indicating that all hydrogen and oxygen in CD have been consumed, and the residual carbon (having relatively low surface energy) may involve in coalescence to form the carbon-shell.

Fig. 2 shows the TEM images of the Co@C nanoparticles. It is clear that the Co nanoparticles are homogeneously dispersed (Fig. 2(a)). The selected-area diffraction (SAD) pattern in Fig. 2(b) is indicative

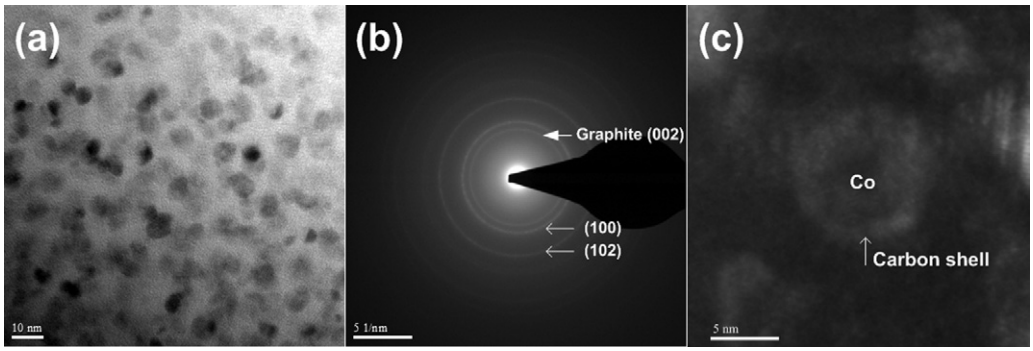

Fig. 2. TEM images of (a) Co@C, (b) corresponding SAD pattern which is indicative of Co (100) and (102) planes, and the innermost ring roughly at the graphite (002) spacing, and (c) the dark-field image that clearly shows the boundary of the carbon-shell and Co nanoparticle carbonized at 573 K.

of the (100) and (102) planes of Co, with the innermost ring roughly at graphite (002) spacing, indicative of amorphous graphite-like carbon phases. The contrast dark-field image in Fig. 2(c) evidently shows the interfacial boundary of the core Co and carbon-shell. The Co has an average size of 5–6 nm in diameter, and the thickness of the coated carbon-shell is in the range of 1.8–2.4 nm.

To better understand growth path of the Co@C nanoparticles during TPC, their *in situ* SAXS patterns were collected with the scattering intensity, *I(q)*, *versus* the scattering vector, ***(q)***. The magnitude of scattering vector, *q*, is defined as $(4\pi/\lambda)sin(\theta/2)$, where λ is the wavelength of the highly collimated and monochromatic X-ray beam, and θ the scattering angle measured for a given sample [34,36,38–40].

For homogeneous particles with average surface area, *S*, the Porod behavior can be applied: $I(q)= 2\pi N\Delta\rho^2 Sq^{-4}$, where *N* is the number density of molecules, and ρ the scattering length density, which is known as the power-law scattering [36]: $I(q) \propto q^{-p}$, where *p* is the power-law exponent, and $3 \leq p < 4$ is indicative of surface fractal. The structure factor, *S(q)*, is a function of *N* and the interaction potential. For relatively low polydispersities of particles with spherical symmetry and narrow size distribution, *I(q)* can be approximated as equation (1):

$$I(q) = NV^2 \Delta\rho^2 \langle P(q)\rangle \left[1 + \frac{\langle F(q)\rangle^2}{\langle F^2(q)\rangle}(S(q) - 1)\right] \quad (1)$$

where *V* is the volume of the particle, *P(q)* the scattering form factor describing the spherical shape of the particle, *F(q)* the coherent sum of the scattering amplitudes of the individual scattering centers within the spherical particle given by the Fourier transform of the electron density distribution, and the angular brackets showing the average quantities over the size distribution. Schultz distribution is the analytical expression for equation (1) [34–36,41]. In this study, the particle sizes of the Co@C were fitted by the SAXS patterns with the Schultz distribution function as polydisperse spheres between q range of 0.01–0.09 $Å^{-1}$, after removing contributions of the background and fractal scattering [34–36].

The *in situ* SAXS spectra of Co obtained at 333 K is fitted by the power law scattering to the slope of -3.9, signaling surface fractal, indicating that the Co^{2+}-CD complex exhibits grains with rough surfaces (see Fig. S1). The growth of the Co nanoparticles during TPC is revealed with the refined SAXS spectra (shown in Fig. 3(a)) by subtracting the scattering intensity *I(q)* at 333 K from each *I(q)* measured between 393–573 K and then fitted with a spherical shape model. The swelling of *I(q)* from 333–393 K at the wave-vector transfer (q = 0.06–0.09 $Å^{-1}$) may be associated with the nucleation of Co reduced from Co(II) (Fig. S1). The increased *I(q)* at 393–423 K reflects the coalescence of adjacent Co particles. At the temperatures of >483 K, the rapid increase of *I(q)* at q = 0.02–0.04 $Å^{-1}$ manifests an increase of the Co nanoparticle size. The increasing *I(q)* at q <0.02 $Å^{-1}$ (at 483–513 K) indicates the total number of the Co nanoparticle is increased. A rapid increase of the most-probable particle diameter (d_p) (in the Schultz distribution) for Co is found between 483–513 K. At 543 K, the size of the Co nanoparticle is slowly increased, and the growth is terminated eventually at 573 K by encapsulation with the carbon-shell since carbon (1.4 J/m^2) has much less surface energy than Co (2.8 J/m^2) [29].

Interestingly, two distinct growth stages are noted with a particle growth transition-state having the Co particle size of about 2.2 nm in diameter at the temperature range of 423–483 K in the

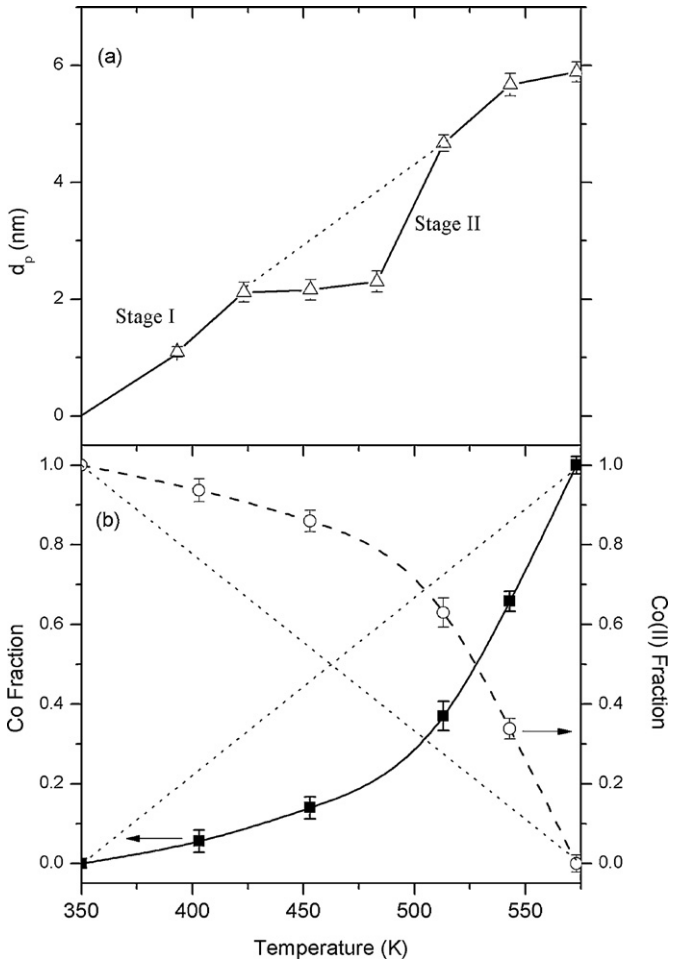

Fig. 3. (a) Growth of Co observed by *in situ* SAXS. d_p denotes the most-probable Co particle size in diameter. (b) Fractions of Co and Co(II) during temperature-programmed carbonization determined by the component-fitted XANES.

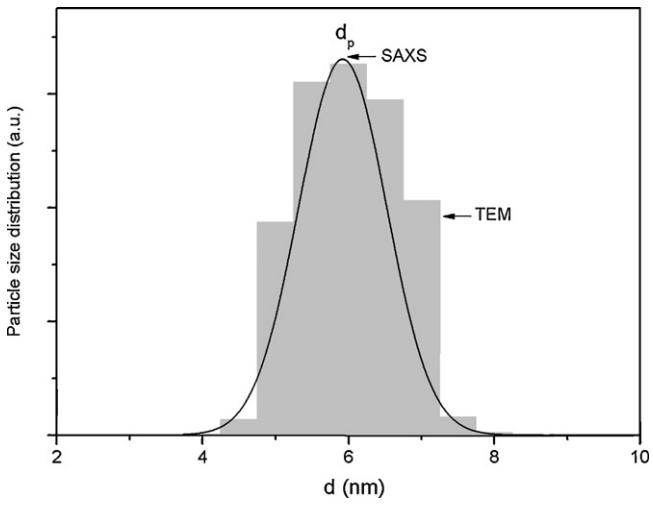

Fig. 4. Particle size distribution of the ripened Co nanoparticle in Co@C carbonized at 573 K obtained from refined SAXS spectra fitted with Schultz distribution (solid line). For comparison, their TEM-derived data are shown in gray bar. Note that d_p is the most-probable particle size in diameter determined by SAXS analysis.

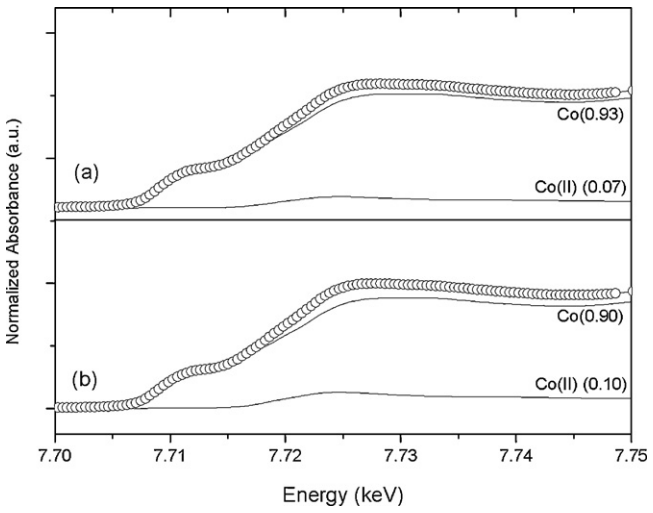

Fig. 5. XANES spectra and the least-squared component fits of (a) Co@C, and (b) steam-reformed Co@C at 573 K for 10 mins. The solid line denotes the spectra of Co and CoO, and the circle denotes fitted sample spectra at R <0.002.

TPC process. At the temperatures of <423 K (stage I) in Fig. 3(a), the d_p for Co increases as the carbonization temperature is increased. A very small amount of carbon and hydrogen in CD involves in oxidation (see Fig. 1), which is coupled with a limited number of Co(II) being reduced (to Co) (see Fig. 3(b)). Nucleation and coalescence of Co may also involve in the stage (I). At the stage II (between 483 and 513 K), a rapid coalescence and fusion of Co nanoparticles proceed as the temperature is increased until the Co nanoparticles are ripened at 573 K. Fig. 4 shows the Schultz distribution of Co nanoparticles in Co@C determined by the SAXS pattern at 573 K. The d_p of the ripened Co is 5.9 nm, being in good agreement with the TEM observations (shown in the gray bar in Fig. 4). The Co growth is terminated by encapsulation with the carbon-shell formed from complete consumption of hydrogen and oxygen in CD, and about 73% of carbon left for the yield of the carbon-shell. The Co growth can be referred to the sequences of (i) nucleation and coalescence of adjacent nanoparticles at 393–413 K (stage I); (ii) a growth transition state for Co nanoparticles having an average d_p of 2.2 nm at 413–483 K; (iii) a rapid fusion of Co nanoparticles at 493–513 K (stage II); and (iv) a ripened Co nanoparticles having a d_p of 5.9 nm at 573 K.

The free small Co_n clusters have stable structures with n = 4, 6, 13, and 19, and as the cluster size increases, the icosahedral structure remains preferentially stable [42,43]. The most stable cluster is obtained by forcing the added atoms on the rigid core of icosahedral sites, known as umbrella model, to minimize the total energy [44]. When a corner and the five surrounding faces are covered, the stability of a cluster is enhanced. For instance, a Co cluster is stable at the 4th shell for n = 216; 5th shell for n = 510 [44]. By assuming the cluster size of Co_{55} = 1.1 nm, Co_{216} = 2.16 nm, and Co_{510} = 4.67 nm, the average growth rates of Co at stages I and II during TCP are about 27 and 98 atoms/min, respectively.

Oxidation state and site geometry of selected element can be revealed by XANES [45]. The XANES spectrum of a sample is composed of the spectra of component compounds by the fractions that made up the sample in a linear relationship [46–48]. Hence, by linearly component-fitting of the XANES spectrum with standard compounds such as Co and CoO, the composition of an unknown sample can be determined [4,49–51]. Fig. 3(b) shows the interconversion of Co(II) to Co, which is derived from the component fitted Co K-edge XANES spectra obtained during TPC at 393–573 K (see Fig. S2 and Fig. 5(a)). It is clear that formation of Co is at the expense of Co(II) disappearance which is attributable to reduction. Note that at the temperatures between 393–483 K, reduction of Co(II) to Co is not very effective, *i.e.*, 8% of Co at 393 K; 20% at 483 K *versus* 93% at 573 K (see Fig. 3(b)). This has implications in that the relatively slow coalescence and fusion of Co nanoparticles at the temperatures of <483 K may be caused by the retarded reduction of Co(II). The carbon-shell may play the major role in prevention of the core Co nanoparticles from aggregation and oxidation.

The ferromagnetic behavior of Co@C was also measured with static magnetization at 300 K. Fig. 6 shows that a zero remanence of the Co@C is found by the hysteresis loop. The hysteresis curve possesses a saturation magnetization (M_s) of 140 emu/g, which is greatly enhanced compared to the values of Co@C (106 emu/g) [25], and the values of $CoFe_2O_4$ (55–64 emu/g) [26]. The enhanced magnetization field of Co@C may be associated with the growth of the crystallographic directions of the Co nanoparticles by reduction of Co^{2+} to Co during TPC.

The steam reforming of the Co@C under 5% of steam at 573 K for 10 minutes was performed to remove the carbon-shell ($C + H_2O \rightarrow CO + H_2$), and thus yield the Co nanoparticles. Fig. 5(b) shows the linear component-fitted XANES spectra of cobalt in the steam-reformed Co@C. About 90% of Co and 10% of CoO are observed

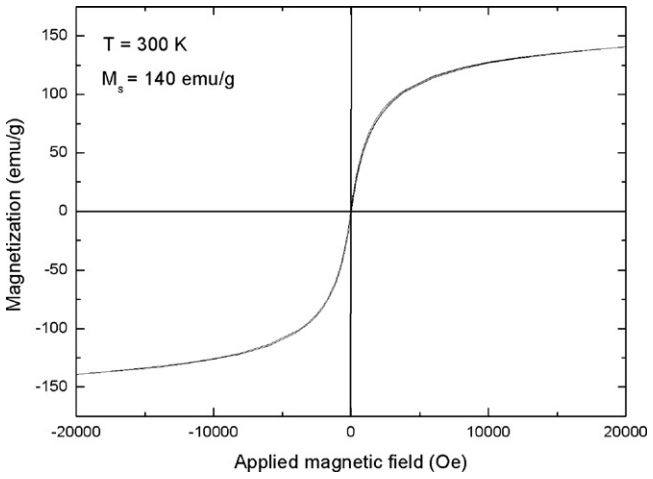

Fig. 6. Magnetization of Co@C having the hysteresis loop at the temperature of 300 K. The saturation magnetization (M_s) of the Co@C nanoparticles is 140 meu/g.

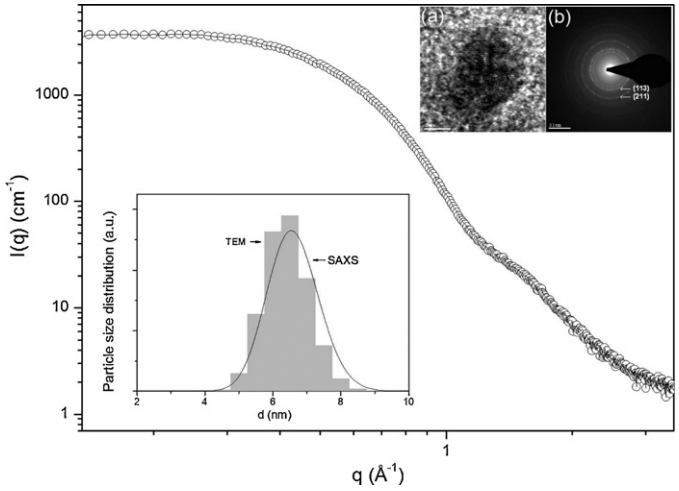

Fig. 7. SAXS pattern of the steam-reformed Co@C. It is clear that the carbon-shell is not found in the steam-reformed Co@C as shown in the TEM images (see the upper inset (a)). The corresponding SAD patterns (upper inset (b)) are indicative of Co (100) and (102) (as shown in Fig. 2(b)) and CoO (113) and (211) planes, suggesting that CoO may coat on the surface of Co nanoparticles after the steam-reforming treatment. Their size distributions were obtained by Schultz distribution of SAXS (line) and TEM (bar), which are in good agreement (shown in the lower inset). The most-probable size (d_p) is 6.3 nm in diameter by SAXS analysis.

after steam reforming. The corresponding SAXS pattern of the steam-reformed Co@C indicates the most-probable size is 6.3 nm in diameter (see Fig. 7), in good agreement with the TEM measurements (see the inset in Fig. 7). The TEM image clearly shows that the carbon-shell is removed, and CoO is found by SAD. It is worth noting that a Co@CoO structure having 90% of Co encapsulated in 10% of CoO shell is formed after the steam-reforming of the Co@C nanoparticle.

4. Conclusions

Two distinct growth stages during TPC of the Co-CD complex at 363–573 K are observed by *in situ* synchrotron SAXS spectroscopy. When CD is carbonized at 393–423 K (stage I), a relatively slow coalescence and fusion of Co nanoparticles at the temperatures of 393–483 K may be caused by the retarded reduction of Co(II), observed by component-fitted XANES. In the stage II at 483–573 K, an increasing Co(II) reduction rate is coupled with a rapid fusion and coalescence of small Co nanoparticles. The stages I and II have the growth rates of 27 and 98 atoms/min, respectively. It is also worth noting that a particle growth transition-state (423–483 K) between the two growth stages has a Co particle diameter of 2.2 nm, which is similar to the size of a stable Co_{261} cluster. The most-probable particle diameter of the Schultz distribution for the ripened Co in Co@C is 5.9 nm. Co@C has a saturation magnetization (M_s) of 140 emu/g. The carbon-shell of the Co@C nanoparticle can be removed by steam reforming to yield desired sizes of Co nanoparticles.

Acknowledgements

The financial supports of the Taiwan National Science Council, Ministry of Economic Affairs (Project #: 101-EC-17-A-10-S1-187), Bureau of Energy, and National Synchrotron Radiation Research Center are gratefully acknowledged. We also gratefully thank Dr. F.C. Chang for assisting the experiments of magnetic properties.

Appendix A. Supplementary data

Supplementary data associated with this article can be found, in the online version, at http://dx.doi.org/10.1016/j.elspec.2012.11.010.

References

[1] F. Lakadamyali, E. Reisner, Chem. Commun. 47 (2011) 1695–1697.
[2] S. Mohapatra, S.R. Rout, S. Maiti, T.K. Maiti, A.B. Panda, J. Mater. Chem. 21 (2011) 9185–9193.
[3] K. Gotoh, T. Kinumoto, E. Fujii, A. Yamamoto, H. Hashimoto, T. Ohkubo, A. Itadani, Y. Kuroda, H. Ishida, Carbon 49 (2011) 1118–1125.
[4] D.J. Sprouster, R. Giulian, L.L. Araujo, P. Kluth, B. Johannessen, D.J. Cookson, M.C. Ridgway, J. Appl. Phys. 109 (2011) 113504.
[5] C.J. Zhong, M.M. Maye, Adv. Mater. 13 (2001) 1507–1511.
[6] X.M. Feng, C.J. Mao, G. Yang, W.H. Hou, J.J. Zhu, Langmuir 22 (2006) 4384–4389.
[7] S. Han, Y. Yun, K.-W. Park, Y.-E. Sung, T. Hyeon, Adv. Mater. 15 (2003) 1922–1925.
[8] F.L. Chen, I.W. Sun, H.P. Wang, C.H. Huang, J. Nanomater. 2009 (2009) 472950.
[9] J. Zhou, H. Song, X. Chen, L. Zhi, J. Huo, B. Cheng, Chem. Mater. 21 (2009) 3730–3737.
[10] J.S. Zhou, H.H. Song, X.H. Chen, L.J. Zhi, S.Y. Yang, J.P. Huo, W.T. Yang, Chem. Mater. 21 (2009) 2935–2940.
[11] L.M. Guo, L.X. Zhang, J.M. Zhang, J. Zhou, Q.J. He, S.Z. Zeng, X.Z. Cui, J.L. Shi, Chem. Commun. (2009) 6071–6073.
[12] J. Robertson, Mater. Sci. Eng. R: Reports 37 (2002) 129–281.
[13] S. Ouyang, H.W. Hsu, L.T. Tong, C.W. Liao, R.Y.Z. Hu, Sustain. Environ. Res. 21 (2011) 21–28.
[14] G. Kickelbick, Prog. Polym. Sci. 28 (2003) 83–114.
[15] M. Marini, M. Toselli, S. Borsacchi, G. Mollica, M. Geppi, F. Pilati, J. Polym. Sci. Pol. Chem. 46 (2008) 1699–1709.
[16] M. Yamada, Bull. Chem. Soc. Jpn. 82 (2009) 152–170.
[17] H. Li, W. Kang, B. Xi, Y. Yan, H. Bi, Y. Zhu, Y. Qian, Carbon 48 (2010) 464–469.
[18] C.-I. Hong, H.-Y. Kang, H.P. Wang, W.-K. Lin, U.S. Jeng, C.-H. Su, J. Electron Spectrosc. Relat. Phenom. 184 (2011) 301–303.
[19] Y. Xu, M. Mahmood, Z.R. Li, E. Dervishi, S. Trigwell, V.P. Zharov, N. Ali, V. Saini, A.R. Biris, D. Lupu, D. Boldor, A.S. Biris, Nanotechnology. 19 (2008) 435102.
[20] I. Sharifi, H. Shokrollahi, S. Amiri, J. Magn. Magn. Mater. 324 (2012) 903–915.
[21] L.M. Lacroix, D. Ho, S.H. Sun, Curr. Top. Med. Chem. 10 (2010) 1184–1197.
[22] A. Lascialfari, C. Sangregorio, Chim. Oggi-Chem. Today. 29 (2011) 20–23.
[23] A.M. Nowicka, A. Kowalczyk, M. Donten, P. Krysinski, Z. Stojek, Anal. Chem. 81 (2009) 7474–7483.
[24] J.D. Gomes, M.H. Sousa, F.A. Tourinho, R. Aquino, G.J. da Silva, J. Depeyrot, E. Dubois, R. Perzynski, J. Phys. Chem. C 112 (2008) 6220–6227.
[25] P. Lukanov, V.K. Anuganti, Y. Krupskaya, A.M. Galibert, B. Soula, C. Tilmaciu, A.H. Velders, R. Klingeler, B. Buchner, E. Flahaut, Adv. Funct. Mater. 21 (2011) 3583–3588.
[26] H.M. Joshi, Y.P. Lin, M. Aslam, P.V. Prasad, E.A. Schultz-Sikma, R. Edelman, T. Meade, V.P. Dravid, J. Phys. Chem. C 113 (2009) 17761–17767.
[27] L. Sciortino, F. Giannici, A. Martorana, A.M. Ruggirello, V.T. Liveri, G. Portale, M.P. Casaletto, A. Longo, J. Phys. Chem. C 115 (2011) 6360–6366.
[28] C. Langlois, D. Alloyeau, Y. Le Bouar, A. Loiseau, T. Oikawa, C. Mottet, C. Ricolleau, Faraday Discuss. 138 (2008) 375–391.
[29] G. Palasantzas, T. Vystavel, S.A. Koch, J.T.M. De Hosson, J. Appl. Phys. 99 (2006).
[30] T.-J. Kühn, W. Caliebe, N. Matoussevitch, H. Bönnemann, J. Hormes, Adv. Organomet. Chem. 25 (2011) 577–584.
[31] C.H. Huang, H.P. Wang, J.E. Chang, E.M. Eyring, Chem. Commun. (2009) 4663–4665.
[32] Y.M. Ciu, C.H. Huang, F.C. Chang, H.Y. Kang, H.P. Wang, Sustan. Environ. Res (2011) 279–282.
[33] D.G. Liu, C.H. Chang, C.Y. Liu, S.H. Chang, J.M. Juang, Y.F. Song, K.L. Yu, K.F. Liao, C.S. Hwang, H.S. Fung, P.C. Tseng, C.Y. Huang, L.J. Huang, S.C. Chung, M.T. Tang, K.L. Tsang, Y.S. Huang, C.K. Kuan, Y.C. Liu, K.S. Liang, U.S. Jeng, J. Synchrot. Radiat. 16 (2009) 97–104.
[34] A. Guinier, G. Fournet, Small-Angle Scattering of X-rays, John Wiley & Sons, New York, 1955.
[35] S.R. Aragon, R. Pecora, J. Chem. Phys. 64 (1976) 2395–2404.
[36] G. Porod, Small Angle X-ray Scattering, Academic Press, New York, 1980.
[37] B. Ravel, M. Newville, J. Synchrot. Radiat. 12 (2005) 537–541.
[38] L.A. Feigin, D.I. Svergun, Structure Analysis by Small-Angle X-ray and Neutron Scattering, New York and London, Plenum, 1987.
[39] G. Beaucage, J. Appl. Crystallogr. 29 (1996) 134–146.
[40] G. Beaucage, J. Appl. Crystallogr. 28 (1995) 717–728.
[41] M. Kotlarchyk, S.H. Chen, J. Chem. Phys. 79 (1983) 2461–2469.
[42] S.D. Borisova, G.G. Rusina, E.V. Chulkov, Phys. Solid State 52 (2010) 838–843.
[43] B.W. Heinrich, L. Limot, M.V. Rastei, C. Iacovita, J.P. Bucher, D.M. Djimbi, C. Massobrio, M. Boero, Phys. Rev. Lett. 107 (2011) 216807.
[44] M. Pellarin, B. Baguenard, J.L. Vialle, J. Lermé, M. Broyer, J. Miller, A. Perez, Chem. Phys. Lett. 217 (1994) 349–356.
[45] K.A. Evans, H.S.C. O'Neill, J.A. Mavrogenes, N.S. Keller, L.Y. Jang, J.F. Lee, Geochim. Cosmochim. Acta 73 (2009) 6847–6867.
[46] F.G. Requejo, J.M. Ramallo-López, R. Rosas-Salas, J.M. Domínguez, J.A. Rodriguez, J.Y. Kim, R. Quijada, Catal. Today 107-108 (2005) 750–758.

[47] S.I. Zabinsky, J.J. Rehr, A. Ankudinov, R.C. Albers, M.J. Eller, Phys. Rev. B 52 (1995) 2995–3009.
[48] T.F. Hsu, T.L. Hsiung, J. Wang, C.H. Huang, H. Paul Wang, Nucl. Instrum. Meth. Phys. Res. A. 619 (2010) 98–101.
[49] C.-Y. Liao, C.-Y. Peng, H.-C. Wang, H.-Y. Kang, H. Paul Wang, Nucl. Instrum. Meth. Phys. Res. A 652 (2011) 925–927.
[50] S.H. Liu, H.P. Wang, C.H. Huang, T.L. Hsiung, J. Synchrotr. Radiat. 17 (2010) 202–206.
[51] Y.P. Sun, X.Q. Li, J.S. Cao, W.X. Zhang, H.P. Wang, Adv. Colloid Interface Sci. 120 (2006) 47–56.